Enhanced output power of freestanding ball-based triboelectric generator through electrophorus effect

*Tsz Hin Choy[1†], Ying Ying O[1†], Feichi Zhou[1], Wei Xu[1], Man Chung Wong[1], Tao Ye[2], Jianhua Hao[1], and Yang Chai[1]**

[1] Department of Applied Physics, The Hong Kong Polytechnic University, Hung Hom, Kowloon, Hong Kong, China.

[2] Department of Electrical and Electronics Engineering, Southern University of Science and Technology

*Correspondence should be addressed to: ychai@polyu.edu.hk

Abstract- Recent development of Internet of Things and related sensor technologies have greatly impacted on the logistics tracking, structural health monitoring, environment analysis, and data extraction. It is highly imperative to develop a technology to allow the sensor node to operate independently, sustainably, and maintenance-free by harvesting the energy from the ambient environment. Here we demonstrate a triboelectric device as a high-efficient and durable kinetic energy harvester from ubiquitously mechanical vibration. We construct a cylinder coated with polytetrafluoroethylene (PTFE), and place a number of metal balls inside the cylinder. This ball-based triboelectric generator (B-TEG) coverts the mechanical shaking into electricity. By grounding the metal-freestanding-layer, we form a new configuration (B-GTEG). The output power of B-GTEG shows 8 times improvement through the electrophorus effect compared with B-TEG, providing potential for supplying sustainable power to wireless sensor nodes.

TOC Figure:

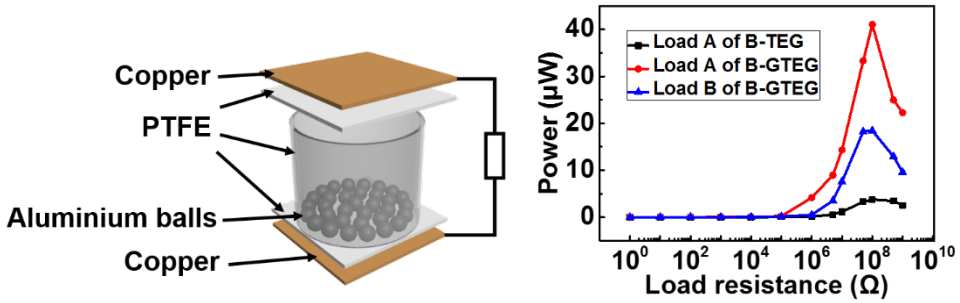

Keywords: Triboelectric nanogenerator; freestanding mode; mechanical shaking; electrophorus effect; Internet of Things

1. Introduction

Wireless sensor networks (WSNs) are widely used in logistics data logging [1], construction health monitoring [2], environment status monitoring [3], and healthcare monitoring [4]. With the limited lifetime of batteries, power source has become a big barrier for further implementation of WSNs. Exploiting sustainable power source from the ambient is the ideal and most demanding challenge for future industries. Energy harvesting devices convert ambient energy sources, such as, solar light [5], mechanical vibrations [6-7], heat [8] etc., into electricity.

Solar cell is a well-developed mature technology for harvesting ambient light and supplying electricity. However, it cannot supply electrical power under the environment without light exposure, which greatly restricts its application scenarios. When sensor nodes are embedded in dark and inaccessible locations, they require sustainable power sources. For example, the containers in the logistics are typically placed inside the trucks and vessels. They lack of solar light but are rich with mechanical vibration during

the transportation. It is important to develop enabling technologies that can harvest kinetic energy to supply power to sensor nodes (inside containers), which are placed without the exposure to solar light. Among all energy sources, mechanical vibration ubiquitously exists in various environments, such as, vibration of machine, human movement, the flow of water and wind [9-13]. Piezoelectric and triboelectric harvester can convert the mechanical motion into electricity [14-16].

Triboelectric nanogenerators have attracted significant attention in recent years because of their simple structure and broad materials selection. When a metal and a dielectric contact to each other, electrons transfer from the metal to the dielectric materials. The surface of dielectric material is negatively charged, and the metal surface is positively charged [17-18]. By connecting two materials with a conductor, a high voltage electricity occurs because of contact electrification and electrostatic induction [19]. There are different types of triboelectric generators, including sliding mode [16,20-23], contact mode [15,20,24-30], single-electrode mode [31-33] and freestanding mode [34-35]. To enhance the energy conversion efficiency, Chun *et al.* boosted the output power by 16 times via an electric double layer effect in a configuration of three-layer system [14]. Kim *et al.* designed a powder-based triboelectric nanogenerator, where a rigid acrylic cylinder contains PTFE powder confined between the two aluminum metal plates [36]. The triboelectric nanogenerator based on pressing and sliding structures cover a wide range of mechanical vibrations. In this work, we design and construct a so-called ball-based triboelectric generator (B-TEG) to harvest the shaking motion and convert it to electricity. To effectively harvest

the shaking motion, we place metal balls inside a cylinder covered with PTFE. This structure enables us to have one more terminal in the middle metal balls for charge exchange.

2. Results and discussions

Figure 1(a) shows the schematic diagram of the ball-based triboelectric generator (B-TEG). A paper cylinder has a height of 3 cm and an inner diameter of 3 cm. The surface of this cylinder is coated with PTFE by double side tape. The Al metal balls with a diameter of 1 mm are placed inside the cylinder. The top and bottom surfaces of PTFE cylinder are coated with Cu thin films as top and bottom electrodes. **Figure 1(b)** and **1(c)** show the top-view and side-view photo of the B-TEG structure.

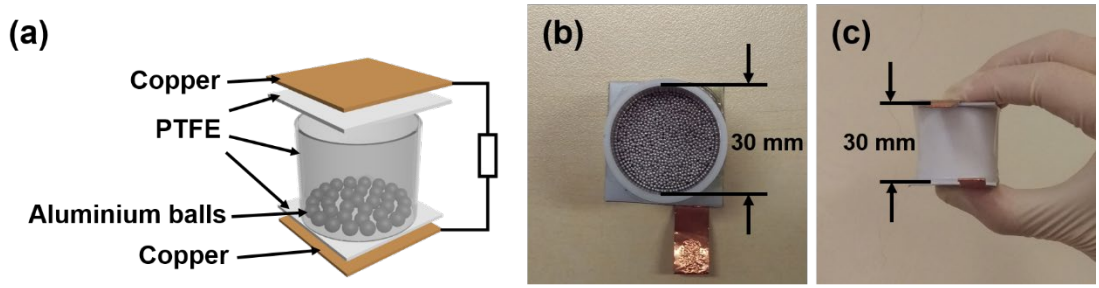

Figure 1. Illustration of the ball-based triboelectric generator. (a) Three-dimension schematic diagram of the ball-based triboelectric generator. Photo of (b) Top view and (c) side view of a ball-based triboelectric generator.

This B-TEG operates in a freestanding mode, in which the Al metal balls serve as a freestanding metal layer and the PTFE cylinder works as the counter triboelectric material. **Figure S1** in the Supplementary Information and **Figure 2** illustrate the working mechanism of ball-based triboelectric generator (B-TEG). In the 1st cycle, as the cylinder with Al balls undergoes mechanical shaking, the inside Al balls contact

(**Figure S1**(a)) with the surface of bottom PTFE and then separate (**Figure 2**(a)) from it. The electrons in Al balls are attracted to PTFE because of triboelectric effect [37]. Thus, the Al balls carry positive charges and PTFE carries negative charges. The positively charged Al balls bring about electrostatic induction to the electrodes near PTFE. The bottom electrode becomes negatively charged [38]. The charges flow through the external circuit and form current (**Figure 2**(b)). Then the Al balls move upward and contact with the surface of top PTFE (**Figure 2**(c)). Similar to the case that the Al balls are contacted with bottom PTFE surface, the contact and separation process generate negative charges on the top Cu electrode, where the direction of current flow is reversed (**Figure 2**(d)). In the whole cycle, the mechanical shaking generates alternating current (AC) in the external circuit of the B-TEG structure, which can be converted to a DC current via a rectifier.

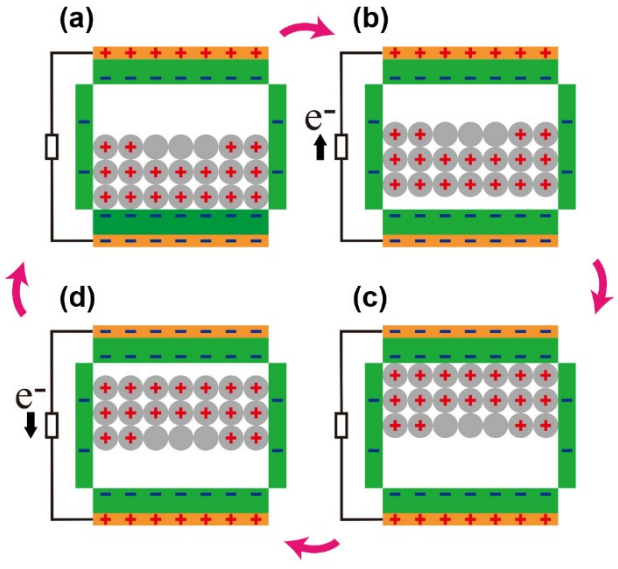

Figure 2. Working mechanism of ball-based triboelectric generator (B-TEG). (a) Contact to bottom surface: Al balls contact with bottom inner surface of PTFE cylinder. (b) Separation from bottom surface: Al balls move upwards and leave the bottom inner surface of PTFE cylinder. (c) Contact to top surface: Al balls contact with the top inner surface of PTFE cylinder.

(d) Separation from top surface: Al balls move downwards and leave the top inner surface of PTFE cylinder.

We use a linear motor (PS-01-37x120-C, LinMot) to provide a mechanical shaking of 1 N force and 3 Hz frequency to the B-TEG. The B-TEG is filled with the Al balls with the volume ratio of 50% and the ball diameter of 1 mm. **Figure 3(a)** shows the two-dimension schematic diagram of the B-TEG, and the open-circuit voltage (V_{OC}) and short-circuit current (I_{SC}) of the B-TEG under external drive are shown in **Figure 3(b)** and **3(c)**. The B-TEG shows high V_{OC} of 26 V, and high I_{SC} of 1.1 μA. We extract the peak power with different load resistors ranging from 1 Ω to 1000 MΩ, as shown in **Figure 3(d)**. The peak power is 22.05 μW with the use of a 500 MΩ load resistor.

We investigate the effect of the volume ratio of Al balls on the output performance of B-TEG. **Figure 3(e)** shows the V_{OC} and I_{SC} of the B-TEG as a function of the volume ratio of the Al balls, from 20% to 80%. When the volume ratio is increased from 20% to 40%, the V_{OC} and I_{SC} is increased from 21.3 V to 27.0 V and from 0.364 μA to 0.557 μA respectively; while the V_{OC} and I_{SC} of B-TEG is decreased when the volume ratio of Al balls is over 40%. With the increase of the volume ratio of Al balls, on one hand, greater contact force will act on the PTFE, which increases the contact area between Al balls and PTFE; on the other hand, the increase of the volume ratio of Al balls decreases the distance between electrodes and Al balls. The electrode, separating from Al balls, is induced negative charges due to a short distance between the electrode and Al balls. The electric potential between two electrodes drops. These two competing factors result in an optimum point. Thus, the output increases with the volume ratio of the Al balls,

but decreases after obtained the maximum output at the volume ratio of 40%.

We also change the ball diameter from 1 mm to 4 mm. **Figure 3(f)** shows that the highest output is obtained using the ball with the diameter of 3 mm. The increase of ball diameter increases the mass of Al ball. The Al balls with low mass have a chance to stick on the inner surface of PTFE cylinder by electrostatic force. The stuck Al balls form a protective wall against the contact of PTFE with other Al balls, and the output voltage and current drops. This problem can be solved using high mass Al balls. On the other hand, the contact area depends on the gap between Al balls. There is a larger gap between Al balls with the increase of ball diameter. Thus, the output of the B-TEG increases with the diameter of balls, while decreases after it reaches the maximum output with the ball diameter of 3 mm. In the rest of the experiments, we use mechanical shaking of 1 N force and 3 Hz frequency, Al ball volume ratio of 50% and ball diameter of 1 mm as a reference to compare with other structures.

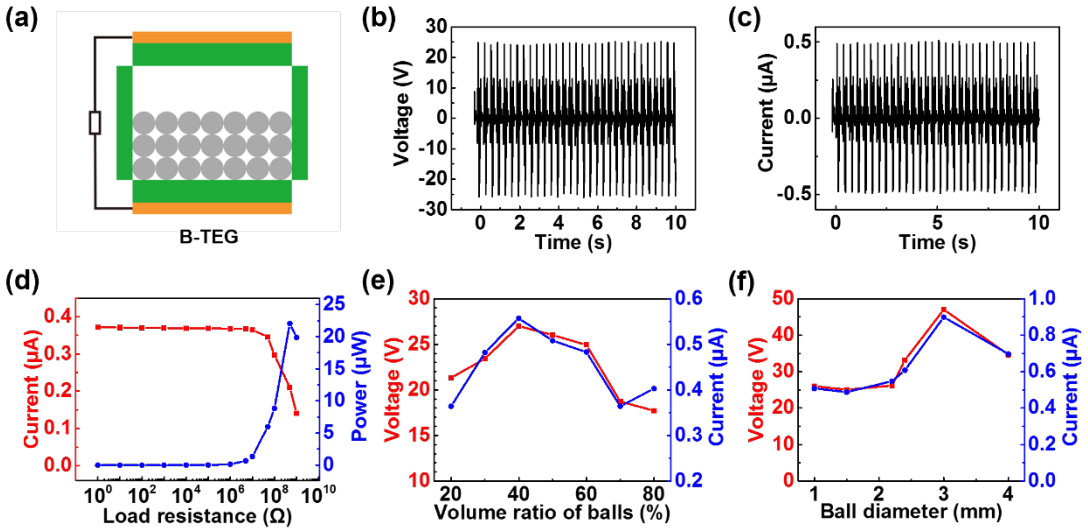

Figure 3. Output performance of ball-based triboelectric generator under a mechanical shaking of 1 N force and 3 Hz frequency. (a) Two-dimension schematic diagram of the ball-based triboelectric generator, (b) open-circuit voltage, (c) short-circuit current, (d) peak power as a function of load resistance, (e) effect of volume ratios of Al balls on the open-circuit voltage

and short-circuit current, and (f) effect of ball diameters of Al balls on the open-circuit voltage and short-circuit current.

In the B-TEG structure, the Al balls inside the container are generated with abundant charges by the triboelectric effect during the shaking motion. But it lacks an effective way to collect the generated charges. To boost the output, we provide one more terminal in the middle of the container, where a metal tape is wrapped around the middle of the inner surface of the container and connected to the ground, as schematically shown in **Figure S2** in the Supplementary Information. The metal tape is a bridge to allow the charge exchange between Al balls and ground during the shaking motion. The charge in Al balls can be extracted by the ground connection for an additional output in this structure. Therefore, a new configuration of grounded-metal-freestanding-layer triboelectric generator (B-GTEG) is designed and created to collect the abundant charges of the Al balls generated during the mechanical shaking, based on Volta's electrophorus.

Figure 4(a) and (b) shows the schematic of B-TEG and B-GTEG. The B-TEG has only one single output (Load A). However, B-GTEG has 2 outputs (Load A and B) because we provide one more terminal of metal tape. We take the Cu metal tape with the width of 5 mm to place in the middle of the cylinder as the additional terminal. The working mechanism of B-GTEG is schematically described in **Figure S3** and **S4** in the Supplementary Information. It is similar to that of B-TEG. The major difference is that the charges in Al balls are allowed to flow to the ground or go back to Al balls by electrophorus effect. When the Al balls approach PTFE, the positive charges and

negative charges in Al balls are separated due to the electrostatic induction of negatively charged PTFE. After the ground connection to the middle terminal of the B-GTEG structure, the Al balls contact with this middle terminal, allowing the negative charges in Al balls to flow to ground. Thus, Al balls become positively charged. This so-called electrophorus effect has been widely used to generate electricity. **Figure 4(c)** shows the peak power of B-TEG and B-GTEG. The Load A of B-GTEG shows much high power of 127.449 μW compared with that of B-TEG (22.05 μW). The total output power of B-GTEG (Load A + Load B) is 178.525 μW. There is an 8-fold output power enhancement. The grounded connection in the middle terminal is needed for electrophorus effect to increases the output current and voltage. Electrophorus effect is used to produce more electrostatic charges in Al balls by electrostatic induction.

We also calculate the average power P_{avg} by this formula [39]:

$$P_{avg} = \frac{\int_{t_0}^{t_0+T} I^2 R dt}{T} \quad (1)$$

where R represents the load resistance, I is the corresponding current, and T is the period of the current waveform. The average power of Load A of B-GTEG also shows a higher output power of 9.9282 μW compared with that of B-TEG (5.93621 μW). The total average power of B-GTEG (Load A + Load B) is 13.14874 μW. B-GTEG still has 2 times output power enhancement in average power.

As the positive charges in Al balls are reduced after connected to the ground, Al balls are easier to lose their electrons to PTFE during the shaking motion. The surface of PTFE becomes more negative. It makes the potential difference between top and bottom electrodes increase. On the other hand, electrophorus effect can be used to

describe the flow of charges in the terminal of metal tape. During the shaking motion, the Al balls contact and separate to inner surface of PTFE cylinder. When the Al balls is approaching to the inner surface of PTFE cylinder, positive charges can be induced to Al balls because of the negative charges on the PTFE surfaces. We can extract more charges from the terminal of metal tape by the electrophorus effect. Thus, the total output power can be enhanced.

We also study the effects of the materials and width of the middle metal tape on the output performance. For Load A, the output current of B-TEG without metal tape is 0.5 μA. After connecting the Al or Cu metal tape in the middle part of the cylinder, the output current of B-GTEG is increased to around 0.9 μA. The structures with grounded metal tapes have a higher output current, as shown in **Figure 4(d)**. The ground connection of metal tape is required for electrophorus effect to extract electrons from Al balls. The output currents of the B-GTEG structure with grounded Al metal tape and Cu metal tape are 1.25 μA and 1.55 μA, respectively. From the table of triboelectric series, Al has a greater tendency to lose electrons than Cu. Al balls becomes more positively charged and have a higher output current after the contact of Al balls and Cu tape.

By increasing the width of the metal tape from 5 mm to 30 mm, the output current is reduced to 1.45 μA (10 mm) and 1.09 μA (30 mm), respectively, as shown in **Figure 4(e)**. The increase of the width of metal tape reduces the contact area of inner surface of PTFE cylinder as well as the accumulated charge in Al balls. As a result, the output power is reduced with the increase of the width of metal tape. The same result is also

shown in Load B, as shown in **Figure 4(f)**. Therefore, the optimized output current can be generated by using grounded Cu metal tape.

To verify the effect of metal tape, we also tried to wrap around the middle of the outer surface of the container by Cu metal tape. However, the output current with outer metal tape is smaller than that without metal tape, as shown in **Figure 4(e) and 4(f)**. Electrophorus effect does not work without a directly ground connection of Al balls. It proves that the metal tape must be connected to Al balls directly to boost the output current.

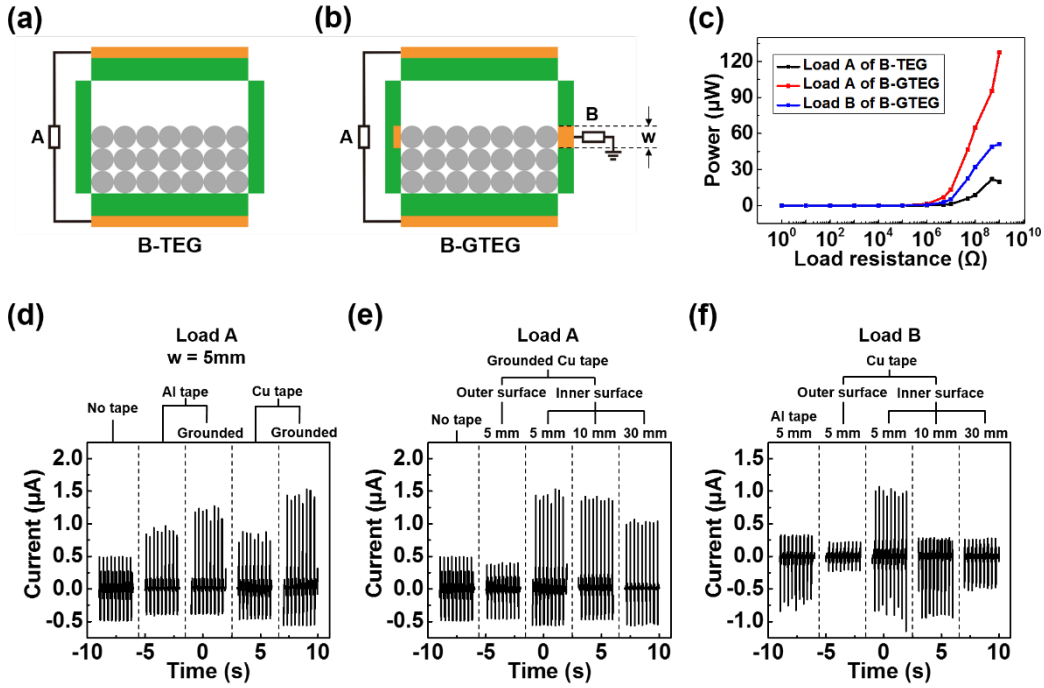

Figure 4. Illustration of the (a) B-TEG and (b) B-GTEG. (c) Peak power of B-TEG and B-GTEG. Short-circuit current with using (d) different materials of metal tape in Load A, (e) different width of metal tape in Load A, (f) different material and width of metal tape in Load B.

The increase in current of B-GTEG is used to compare with other boosting methods of TENG as shown in **Table 1**. The use of grounded-metal-freestanding-layer in B-GTEG has the highest percentage change of current and the output current increases 4

times. The other boosting methods using hybrid mode, molecular surface functionalization, nanopattern and ionized-air injection also have a significant increase in current. A triboelectric nanogenerator (TENG) and an electromagnetic induction generator (EMIG) are integrated into one structure [40]. There is an additional output current generated by the EMIG. The output current increases 37.5% to compare with a single TENG. Molecular surface functionalization is also used to boost the output of TENG [41]. Amine ($–NH_2$) functional group is brought onto an Au film to increase the tendency to lose electrons. It has a 105.56% current increase in TENG. Nanopattern is usually used on the materials of the TENG to increase the contact area of the materials for boosting the output current. A nanomeshes [42] and a pyramid-featured nanopattern [43] are created on the materials. It results a 154.55% and 288.89% current increase in the TENG respectively. Surface charge density limits the output current of the TENG. The maximum surface charge density of a dielectric material can be achieved by injection of ions with an air ionization gun [44]. The output current is increased by 333.33% after maximum surface charge density is achieved. However, they cannot achieve a four-fold increase. The method of grounded-metal-freestanding-layer is provided as the cheapest and most effective method to boost the output current of triboelectric generator.

Table 1. The comparison of percentage change of current by different boosting method of triboelectric generator.

Boosting method	Original Current	Boosted Current	% Change
Grounded-metal-freestanding-layer	0.401 μA	2.119 μA	+428.43%
Hybridizing	1.6 mA	2.2 mA	+37.5%

Triboelectrification and Electromagnetic Induction Effects [40]			
Molecular Surface Functionalization [41]	9 mA/m^2	18.5 mA/m^2	+105.56%
Nanomeshes Block Copolymer TENG [42]	1.1 mA/m^2	2.8 mA/m^2	+154.55%
Pyramid-featured nanopattern TENG [43]	0.18 μA	0.7 μA	+288.89%
Maximum Surface Charge Density for Triboelectric Nanogenerators by Ionized-Air Injection [44]	18 mA	78 mA	+333.33%

The ambient mechanical vibration is usually intermittent and unpredictable. It is important to store the harvested energy in an energy storage device. To harvest the mechanical energy for powering a sensor node, we use a 100 μF capacitor to test the performance of B-TEG and B-GTEG. **Figure 5(a) and (b)** shows the circuit configurations of B-TEG and B-GTEG to charge a capacitor using different number of rectifiers. Capacitor charging curves of different configurations of B-TEG in 100 s are shown in **Figure 5(c)**. B-GTEG has a better performance and it can charge up the capacitor to 0.86 V in 100 s. B-TEG only charge up the capacitor to 0.49 V in 100 s. **Figure 5(d)** shows that B-GTEG can light up 100 LEDs.

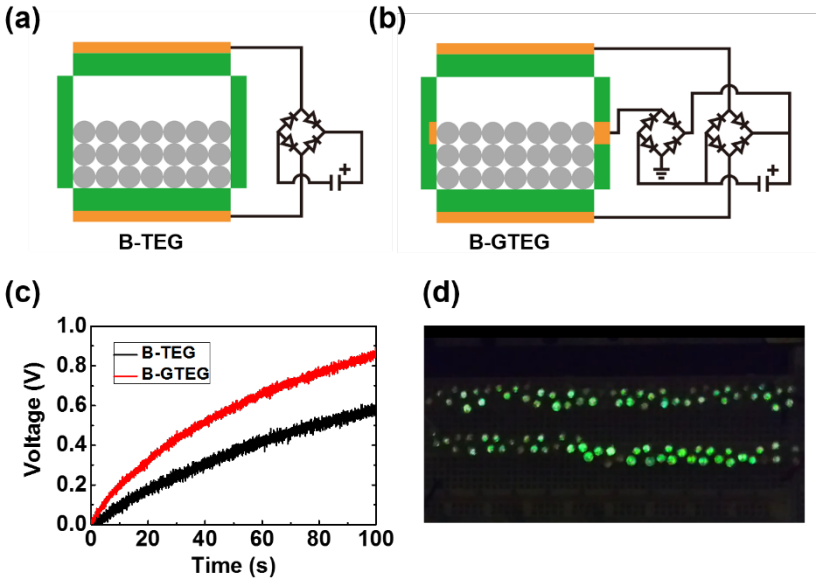

Figure 5. The circuit diagram of charging capacitor in (a) B-TEG and (b) B-GTEG. (c) Plot of 100uF capacitor charging with B-TEG and B-GTEG in 100 s. (d) Photo of lighting up 100 LEDs by B-GTEG under dark environment.

3. Methods

3.1 Fabrication of Copper thin film electrodes on a piece of dielectric material

PTFE (PTFE, Huasheng) with 1 mm thickness was used as dielectric material. To prepare a coated PTFE sample, the air gun was used to remove the dust. The cleared PTFE was put into MRC sputter with the vacuum at 6 millitorr. The copper was sputtered on the PTFE under 20 sccm Ar flow-rate and 70 W Power for 15 min. The thickness of copper layer is around 70 nm on the one side of PTFE, used as the top and bottom layers.

3.2 Fabrication of triboelectric generator

A piece of PTFE was bended as a cylinder which have 30 mm diameter and 30 mm height. The copper tape with 5 mm width was stuck around the inner surface of the

PTFE cylinder in the middle position. The bottom layer, which is a piece of 3.6 cm x 3.6 cm PTFE with copper coating, was used to cover one of sides of cylinder. Different numbers of 1 mm Al metal balls were put into the cylinder before it was sealed by another piece of PTFE with copper coating.

3.3 Characterization and measurements

A linear motor (PS-01-37x120-C, LinMot) which was operated at a cycle of cosine curve and 154 ms at rest was used to create a 3 Hz and 1 N shaking motion to the triboelectric generator. The period of cosine curve is 179.3 ms and the peak to peak value is 30 mm. A 600 MHz Oscilloscope (WaveSurfer 62Xs, LeCroy) and a low-noise current preamplifier (Model SR570, Stanford Research Systems, Inc.) were used for electrical measurements.

4. Conclusion

In summary, we design and construct a freestanding ball-based triboelectric generator and create a grounded metal-freestanding-layer. Cu tape is used as the bridge to connect Al balls to the ground. The B-GTEG can boost the output power by the Cu-Al interaction and electrophorus effect. The output power is increased from 22.05 μW (B-TEG) to 178.525 μW (B-GTEG). There is an 8-fold output power enhancement. Grounded metal-freestanding-layer is an easy way to boost a freestanding triboelectric generator. Our works provide great advantages over conventional power boost method on triboelectric generator.

Acknowledgements

This work was supported by the Hong Kong Polytechnic University (Grant No.: 5-ZG6C).

References:

[1] L. Jin, W. Deng, Y. Su, Z. Xu, H. Meng, B. Wang, H. Zhang, B. Zhang, L. Zhang, X. Xiao, M. Zhu and W. Yang, *Nano Energy*, 2017, **38**, 185-192.

[2] H. Yu, X. He, W. Ding, Y. Hu, D. Yang, S. Lu, C. Wu, H. Zou, R. Liu, C. Lu and Z. L. Wang, *Advanced Energy Materials*, 2017, **7**, DOI: 10.1002/aenm.201700565.

[3] Z. Li, J. Chen, J. Zhou, L. Zheng, K. C. Pradel, X. Fan, H. Guo, Z. Wen, M. H. Yeh, C. Yu and Z. L. Wang, *Nano Energy*, 2016, **22**, 548-557.

[4] P. Bai, G. Zhu, Q. Jing, J. Yang, J. Chen, Y. Su, J. Ma, G. Zhang and Z. L. Wang, *Advanced Functional Materials*, 2017, **24**, 5807–5813.

[5] F. Zhou, Z. Ren, Y. Zhao, X. Shen, A. Wang, Y. Y. Li, C. Surya and Y. Chai, *ACS Nano*, 2016, **10**, 5900-5908.

[6] R. Song, H. Jin, X. Li, L. Fei, Y. Zhao, H. Huang, H. L. Chan, Y Wang and Y. Chai, *Journal of Materials Chemistry*, 2015, **3**, 14963-14970.

[7] B. Ahmed-Seddik, G. Despesse, S. Boisseau and E. Defay, *Journal of Physics: Conference Series*, 2013, **476**, 012069.

[8] M. Hyland, H. Hunter, J. Liu, E. Veety and D. Vashaee, *Applied Energy*, 2016, **182**, 518-524.

[9] Z. H. Lin, G. Cheng, S. Lee K. C. Pradel and Z. L. Wang, *Advanced Materials*, 2014, **26**, 4690–4696.

[10] X. S. Meng, Z. L. Wang and G. Zhu, *Advanced Materials*, 2016, **28**, 668–676.

[11] S. Lee, W. Ko, Y. Oh, J. Lee, G. Baek, Y. Lee, J. Sohn, S. Cha, J. Kim, J. Park and J. Hong, *Nano Energy*, 2015, **12**, 410-418.

[12] E. Romero-Ramirez, PhD Dissertation, Michigan Technological University, 2010.

[13] S. Li, J. Yuan and H. Lipson, *Journal of Applied Physics*, 2011, **109**, 026104.

[14] J. Chun, B. U. Ye, J. W. Lee, D. Choi, C. Kang, S. Kim, Z. L. Wang and J. M. Baik, *Nature Communications*, 2016, **7**, 12985.

[15] G. Zhu, Z. Lin, Q. Jing, P. Bai, C. Pan, Y. Yang, Y. Zhou and Z. L. Wang, *Nano Letters*, 2013, **13**, 847-853.

[16] S. Niu, Y. Liu, S. Wang, L. Lin, Y. S. Zhou, Y. Hu and Z. L. Wang, *Advanced Materials*, 2013, **25**, 6184–6193.

[17] X. Z. Wang, B. Yang, J. Q. Liu, Y. B. Zhu, C. S. Yang and Q. He, *Scientific Reports*, 2016, **6**, 36409.

[18] Y. L. Zi, C. S. Wu, W. B. Ding and Z. L. Wang, *Advanced Functional Materials*, 2017, **27**, DOI: 10.1002/adfm.201700049.

[19] F. Fan, Z. Tian and Z. L. Wang, *Nano Energy*, 2012, **1**, 328-334.

[20] Z. L. Wang, *ACS Nano*, 2013, **7**, no. 11, 9533-9557.

[21] Y. Yang, H. Zhang, J. Chen, Q. Jing, Y. S. Zhou, X. Wen and Z. L. Wang, *ACS Nano*, 2013,

7, 7342-7351.
[22] Z. L. Wang, L. Lin, J. Chen, S. Niu and Y. Zi, in *Triboelectric Nanogenerators*, Springer, Cham, 2016, pp. 49-90.
[23] G. Zhu, Y. S. Zhou, P. Bai, X. S. Meng, Q. Jing, J. Chen and Z. L. Wang, *Advanced Materials*, 2014, **26**, 3788–3796.
[24] Z. Zhao, X. Pu, C. Du, L. Li, C. Jiang, W. Hu and Z. L. Wang, *ACS Nano*, 2016, **10**, 1780-1787.
[25] Z. L. Wang, L. Lin, J. Chen, S. Niu and Y. Zi, in *Triboelectric Nanogenerators*, Springer, Cham, 2016, pp. 23-47.
[26] H. Fang, H. Tian, J. Li, Q. Li, J. Dai, T. Ren, G. Dong and Q. Yan, *Nano Energy*, 2015, **20**, 48-56.
[27] W. Xu, L. Huang and J. Hao, *Nano Energy*, 2017, **40**, 399-407.
[28] W. Xu, L. Huang, M. Wong, L. Chen, G. Bai and J. Hao, *Advanced Energy Materials*, 2017, **7**, 1601529.
[29] L. Huang, W. Xu, G. Bai, M. Wong, Z. Yang and J. Hao, *Nano Energy*, 2016, **30**, 36-42.
[30] D. Kim, S. Jeon, J. Y. Kim, M. Seol, S. O. Kim and Y. Choi, *Nano Energy*, 2015, **12**, 331-338.
[31] S. S. Kwak, S. Lin, J. H. Lee, H. Ryu, T. Y. Kim, H. Zhong, H. Chen and S. Kim, *ACS Nano*, 2016, **10**, 7297-7302.
[32] Q. Liang, X. Yan, Y. Gu, K. Zhang, M. Liang, S. Lu, X. Zheng and Y. Zhang, *Scientific Reports*, 2015, **5**, 9080.
[33] H. Fang, X. Wang, Q. Li, D. Peng, Q. Yan and C. Pan, *Advanced Energy Materials*, 2016, **6**, 1600829.
[34] S. Niu and Z. L. Wang, *Nano Energy*, 2015, **14**, 161-192.
[35] M. Yeh, H. Guo, L. Lin, Z. Wen, Z. Li, C. Hu and Z. L. Wang, *Advanced Functional Materials*, 2015, **26**, 1054-1062.
[36] D. Kim, Y. Oh, B. Hwang, S. Jeon, S. Park and Y. K. Choi, *ACS Nano*, 2015, **10**, 1017-1024.
[37] M. Lungu, *Minerals Engineering*, 2004, **17**, 69-75.
[38] S. Niu, Y. Liu, X. Chen, S. Wang, Y. S. Zhou, L. Lin, Y. Xie, Z. L. Wang, *Nano Energy*, 2015, **12**, 760-774.
[39] L. Xu, T. Jiang, P. Lin, J. J. Shao, C. He, W. Zhong, X. Y. Chen, Z. L. Wang, *ACS Nano*, 2018, **12**, 1849-1858.
[40] Y. Hu, J. Yang, S. Niu, W. Wu and Z. L. Wang, *ACS Nano*, 2014, **8**, 7442-7450.
[41] S. Wang, Y. Zi, Y. S. Zhou, S. Li, F. Fan, L. Lin and Z. L. Wang, *Journal of Materials Chemistry A*, 2016, **4**, 3728-3734.
[42] C. K. Jeong, K. M. Baek, S. Niu, T. W. Nam, Y. H. Hur, D. Y. Park, G. Hwang, M. Byun, Z. L. Wang, Y. S. Jung and K. J. Lee, *Nano Letters*, 2014, **14**, 7031-7038.
[43] F. Fan, L. Lin, G. Zhu, W. Wu, R. Zhang and Z. L. Wang, *Nano Letters*, 2012, **12**, 3109-3114.
[44] S. Wang, Y. Xie, S. Niu, L. Lin, C. Liu, Y. S. Zhou and Z. L. Wang, *Advanced Materials*, 2014, **26**, 6720-6728.